PAPER

Fabrication of Au nanotube arrays and their plasmonic properties†

Haojun Zhu,[a] Huanjun Chen,[ab] Jianfang Wang[a] and Quan Li[*a]

Large-scale Au nanotube arrays on ITO/glass with tunable inner diameters and wall thicknesses were fabricated *via* a CdSe nanotube array templating method. The initial tubular morphology of the CdSe-nanotube template was maintained during the synthesis, while the composition was converted from CdSe to Au. The obtained Au nanotube arrays showed two surface plasmon resonances in the extinction spectrum, mainly contributed by electron oscillation along the transverse and the longitudinal directions. When used as the substrate for surface-enhanced Raman spectroscopy (SERS), the Raman scattering of the probe molecules (4-mercaptobenzoic acid) was amplified by approximately 4 orders of magnitude, mainly due to the plasmonic enhancement effect of the Au nanotube arrays.

Introduction

The localized surface plasmon resonances (LSPRs) of gold nanostructures enable the manipulation of electromagnetic energy at the subwavelength scale, making nanogold extremely attractive for a wide range of photonic applications. The plasmonic behavior of gold nanostructures (*e.g.*, the resonance energy and the full width at half-maximum (FWHM) of LSPR peaks) is highly sensitive to their size, shape, composition and surrounding medium.[1,2] In the simplest case of small spherical nanoparticles, surface plasmon is dominated by dipolar resonance mode. The anisotropy of nonspherical nanoparticles (*e.g.*, nanorods, nanorings, nanocages and nanostars) leads to multiple LSPR modes and thus provides an opportunity for finely tailoring the optical properties over a broad spectral range without sacrificing the FWHM of the resonance.[3–5] Among various anisotropic Au nanostructures, Au nanotubes are of particular interest. Their plasmonic properties can be manipulated throughout a board spectral range by controlling their inner diameter and tube wall thicknesses.[6,7] The radiation damping can be suppressed in the nanotubes (*vs.* that of the nanorods of the same outer diameter and length), due to the reduced volumes.[8,9] This extends the strength of the local field enhancement around the nanotubes. In addition, the large surface-area-to-volume ratio

of nanotubes is beneficial for a number of sensing applications including biosensing and surface-enhanced Raman spectroscopy (SERS).[10–13]

A few methods are currently available for fabricating Au nanotube arrays. Almost all of them employ either anodic alumina (AAO) or a track-etched polycarbonate membrane as the templates. One strategy is to decorate the pore walls of the template with Sn^{2+}/Ag or silane first so that gold prefers to deposit on the pore walls during the following electrochemical or chemical bath deposition, forming nanotube morphology.[10,14–21] Another strategy involves filling the pores of the template with other materials (*e.g.*, Ni, polypyrrole, polyaniline, *etc.*) first. Then an annular space between the prefilled materials and the template is created by either etching the template pore walls or shrinking the prefilled material (*e.g.* polyaniline). Then electrodeposition of Au in the created annular space would result in the formation of Au nanotubes.[7,13,22–24] Other methods include multistep template replication,[25] shadow evaporation,[12] *etc.* All these previous methods are rather complicated and the Au nanotube arrays synthesized are usually opaque, which limits their applications.

In the present work, we provide an alternative synthetic method that results in semitransparent vertical-aligned Au nanotube arrays on an ITO/glass substrate, by taking CdSe nanotube arrays as the sacrificial template. The inner diameters, tube wall thickness, and the length of the Au nanotube arrays are inherited from those of the CdSe nanotube arrays, which is controllable. The obtained Au nanotube arrays showed two surface plasmon resonances in the extinction spectrum. When taking the Au nanotube arrays on ITO/glass as the SERS substrate, enhancement of the Raman signals of 4-mercapto-benzoic acid (4-MBA) is estimated to be about 4×10^4, consistent with the reported average enhancement factors of other Au nanostructures.[26–29]

[a]*Department of Physics, The Chinese University of Hong Kong, Shatin, New Territories, Hong Kong. E-mail: liquan@phy.cuhk.edu.hk; Tel: +852 39436323*

[b]*State Key Laboratory of Optoelectronic Materials and Technologies, Guangdong Province Key Laboratory of Display Material and Technology, School of Physics and Engineering, Sun Yat-sen University, Guangzhou 510275, China*

† Electronic supplementary information (ESI) available: Basic characterizations, optical and SERS properties of Au nanotube arrays obtained from CdSe nanowire arrays; SERS spectra of Au-sputtered ITO/glass and bare ITO/glass; the calculation details of the enhancement factor. See DOI: 10.1039/c3nr33658a

Experimental details

The CdSe nanotube arrays were synthesized *via* a ZnO nanorod template method, the details of which can be found in the previous studies.[30] Briefly, CdSe nanoshells were electrodeposited on the surface of ZnO nanorods from an aqueous electrolyte solution galvanostatically (at ~1 mA cm^{-2}) at room temperature in a two-electrode electrochemical cell, with the ZnO nanorod-array-on-ITO as the cathode and Pt foil as the anode. The deposition electrolyte contains 0.05 M $Cd(CH_3COO)_2$, 0.1 M Na_3NTA (nitrilotriacetic acid trisodium salt), and 0.05 M Na_2SeSO_3 with excess sulfite.[31,32] After ~7 min of electrodeposition, the ZnO–CdSe nanocable arrays were dipped into a 25% ammonia solution at room temperature for 30 min to remove the ZnO core, forming CdSe nanotube arrays on ITO. Finally, the CdSe nanotube arrays were immersed in 1 mM $HAuCl_4$ and 1.5 mM K_2CO_3 aqueous solution (aged for 1 h) at room temperature for 30 min, completely converting CdSe nanotube arrays into Au nanotube arrays on ITO.

Au nanotube arrays were also synthesized using CdSe nanowire arrays on Ni foil as the template. CdSe nanowire arrays were synthesized by electrodepositing CdSe crystals in the pores of an alumina oxide membrane (AAO, Whatman, Anodisc 13, 0.2 μm) using similar deposition parameters (1 mA, ~8 min) as described above. Next, AAO was removed by the 10% NaOH solution for 20 min and CdSe nanowire arrays were obtained. Then, the surface of CdSe nanowires were converted to Au by immersing them in 5 mM $HAuCl_4$ and 7.5 mM K_2CO_3 aqueous solution for 10 min. Finally, the CdSe core was etched away by 10% HCl solution for 60 min and then by hot 1 M Na_2SO_3 solution for 60 min.

The general morphology of the Au nanotube arrays was examined by scanning electron microscopy (SEM; Quantum F400). Their detailed microstructure and chemical composition were investigated using a transmission electron microscope and a scanning transmission electron microscope (TEM and STEM; Tecnai 20 FEG) equipped with an energy-dispersive X-ray (EDX) spectrometer. Optical extinction spectra were recorded using a Hitachi U3501 spectrophotometer. The optical scattering images of the nanotubes were taken using a color digital camera (Carl Zeiss AxioCam MRC5) attached to an Olympus BX60 optical microscope. The scattering spectra were collected on another Olympus BX60 microscope equipped with a monochromator (Acton SpectraPro 2300i) and a thermoelectrically cooled CCD (Princeton Instruments Pixis 512B). In order to perform surface-enhanced Raman spectroscopy (SERS) measurements, the Au nanotube arrays were first immersed in the aqueous solution containing 1 mM 4-mercaptobenzoic acid (4-MBA) and 0.1 M NaOH for 20 min, then rinsed with clean DI water and ethanol and dried. Two control samples, *i.e.*, 4-MBA-coated ITO/glass and 4-MBA-coated Au thin film on ITO by sputtering were prepared through the same route. Raman measurements were then performed directly on the samples using an EZRaman-M-785 Raman spectrometer (Enwave Optronics, Inc.). The excitation laser wavelength was 785 nm. FDTD simulations were performed on Au nanotubes using FDTD Solutions (Lumerical Solutions, Inc.). The dielectric function of Au was described using the Drude model[5] and the refractive index of the surrounding medium was set to be 1.0 for vacuum. The transverse or longitudinal plasmon resonance were calculated by setting the electric field of the electromagnetic plane wave perpendicular or parallel to the length direction of Au nanotubes, respectively.

Results and discussions

Morphology, crystalline structure, and chemical composition

The Au nanotube arrays were synthesized using CdSe nanotubes as the template. Fig. 1a and b show the SEM images of typical CdSe nanotube arrays on ITO before and after immersing in the $HAuCl_4$ aqueous solution. The inner diameters and wall thicknesses of the CdSe nanotubes are estimated to be 60–80 nm and 20–30 nm, respectively. After being soaked into $HAuCl_4$ solution, the tubular morphology remains intact, with the inner diameter and wall thicknesses of the nanotube barely changed. A more detailed observation of the tubular structure (after $HAuCl_4$ solution treatment) is made using TEM. Fig. 1c shows such a nanotube, in which the patch-like contrast suggests its polycrystalline nature. The grain contrast is also observed in the corresponding high angle annular dark field (HAADF) image (Fig. 1d), in which the strong light contrast results from the large atomic number of Au. The selected-area diffraction (SAD) pattern taken from a single nanotube (Fig. 1e) shows ring patterns that can be indexed to face-centered cubic (fcc) Au, suggesting the obtained nanotube is single-phase polycrystalline Au without the residual CdSe template. A high resolution image (Fig. 1f) taken from a typical grain in the nanotube shows the lattice fringes with hexagonal symmetry, and the measured *d*-spacing is ~0.24 nm, consistent with the
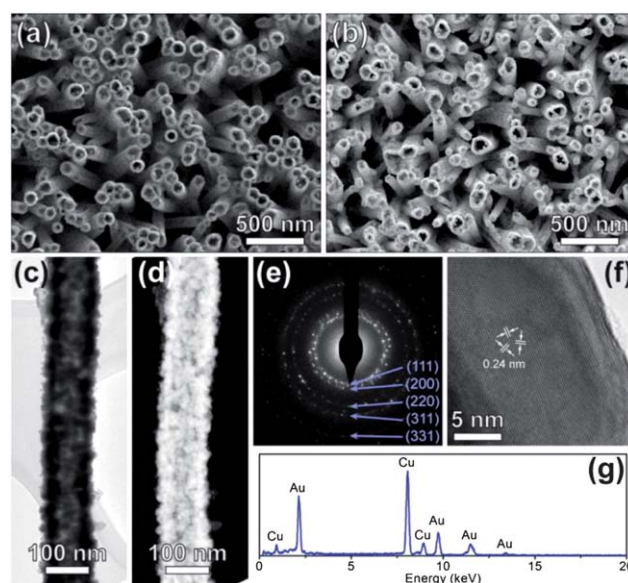

Fig. 1 SEM images of typical CdSe nanotube arrays on ITO/glass (a) before and (b) after immersing in the $HAuCl_4$ aqueous solution. (c) The bright field low-magnification TEM image of single Au nanotube. (d) The HAADF image taken from the same nanotube. (e) The SAD pattern taken from part of the Au nanotube. (f) High resolution image showing a grain of Au in the nanotube. (g) The EDX spectrum taken from the same Au nanotube.

Au $\{1\bar{1}0\}$ spacing. EDX analysis of the nanotube shows that it is composed of Au only, without detectable Cd and Se (Fig. 1g; the Cu signals in the EDX spectrum comes from the TEM grids).

Obviously, the morphology of the Au nanotube is inherited from the CdSe nanotube template. As the size (inner diameter and wall thickness) of the CdSe nanotubes is tunable,[30] control over the size of the Au nanotubes is straightforward. Fig. 2 gives two examples of Au nanotubes formed using CdSe nanotubes with inner diameters of ~200 nm and ~100 nm and wall thicknesses of ~150 nm and ~30 nm, respectively.

In fact, the fabrication process of the Au nanotubes can be simplified by using CdSe nanowires obtained by electroplating (without participation of ZnO). Despite the nanowire morphology of CdSe, it also serves as an effective template for the Au nanotube fabrication (ESI, Fig. S1 and S2†), sharing a similar formation mechanism to the Au nanotubes grown on the CdSe nanotube template.

Au nanotube formation mechanism

The Au nanotube arrays are formed by the redox reaction between an Au(III) salt precursor (i.e., HAuCl$_4$) and CdSe nanotube arrays, which serves as both the reducing agent and template. Due to the strong oxidation ability of $AuCl_4^-$ ions in the aqueous solution, the CdSe crystals on the nanotube are oxidized into SeO_3^{2-} (or SeO_4^{2-}) and dissolved in the solution together with the Cd^{2+} ions. At the same time, the $AuCl_4^-$ ions are reduced to Au^0 and form small Au particles on the CdSe surface. Therefore, CdSe will be slowly etched and replaced by Au crystals, forming Au–CdSe composite nanotubes. By elongating the reaction time, the entire CdSe nanotube template will be consumed and converted to pure Au nanotubes. A similar formation mechanism of noble metal (e.g., Au, Ag, Pt, and Pd) nanostructures taking advantage of the redox reactions has been found in studies using Se, Te, CdSe, CdTe, PbSe and LiMo$_3$Se$_3$ nanostructures as the templates.[33–38]

Fig. 3 shows the characterizations of the Au–CdSe composite nanotubes before the CdSe template is completely consumed. The SEM image (Fig. 3a) discloses its similar morphology to the untreated CdSe nanotube arrays. A hollow tubular morphology can also be seen in both bright field and HAADF TEM images (Fig. 3b and c) taken from a typical single nanotube. The rough surface and patch-like contrast suggest the polycrystalline
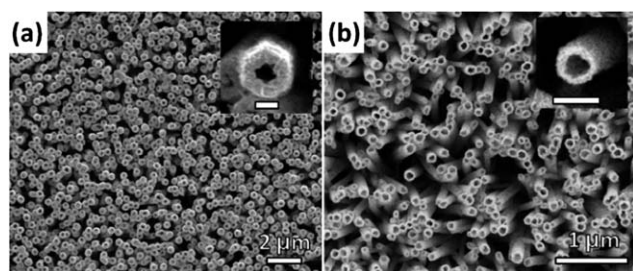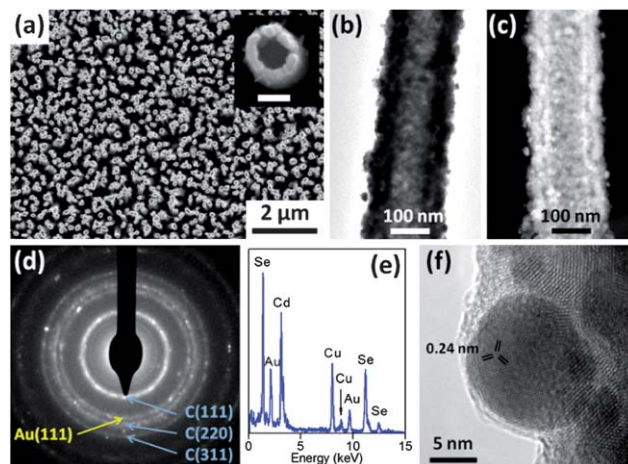

Fig. 3 (a) The SEM image of typical Au–CdSe composite nanotube arrays on ITO/glass; the inset in panel (a) shows the magnified SEM image of a single nanotube (scale bar, 100 nm). (b) The bright field and (c) HAADF TEM images, (d) the SAD pattern and (e) the EDX spectrum taken from a single composite nanotube. (f) HRTEM image showing the lattice fringe of an fcc Au crystal.

nature of the nanotube. The SAD pattern taken from the same nanotube (Fig. 3d) consists of both ring patterns from fcc Au and zinc blende (ZB) CdSe, consistent with its polycrystalline and multi-component nature. EDX analysis of the nanotube shows that it is composed of Cd, Se and Au, with a Cd to Se ratio approximately equal to 1 (Fig. 3e). The SAD and EDX results suggest that the CdSe template is etched close to their stoichiometric ratio and does not form byproducts (e.g., Cd or Se elemental crystals) on the nanotubes. The high-resolution TEM (HRTEM) image taken at the edge of the Au–CdSe composite nanotubes (Fig. 3f) shows an Au nanoparticle having the lattice fringes observable from the Au [111] zone axis.

Plasmonic properties of Au nanotube arrays on ITO/glass substrate

Fig. 4a and b show colored dark-field images of CdSe nanotube arrays and Au nanotube arrays taken at the same magnification and exposure condition, respectively. The dark-field image of CdSe nanotube arrays (Fig. 4a) looks rather dim and is difficult to recognize any features. In contrast, bright golden spots can be seen in the dark-field image of Au nanotube arrays (Fig. 4b), which indicates an enhanced light scattering from the Au nanotube arrays. The scattering spectra obtained from these two nanotube arrays (Fig. 4c and d) reveal a 5–15-fold increase in scattering intensity of Au nanotube arrays than that of CdSe nanotube arrays. Nevertheless, the peaks in the scattering spectrum of Au nanotube arrays are rather broad and individual plasmon peaks can hardly be distinguished. This is mainly due to two reasons, first of all, the high density of Au nanotubes in the array on ITO would lead to coupling of the localized surface plasmons among the adjacent nanotubes causing the broadening of the plasmon peak;[26] secondly, the non-identical sizes and orientation distributions of the nanotubes result in an averaged signal being collected. The extinction spectrum of CdSe nanotube arrays (Fig. 4e) discloses a strong visible light
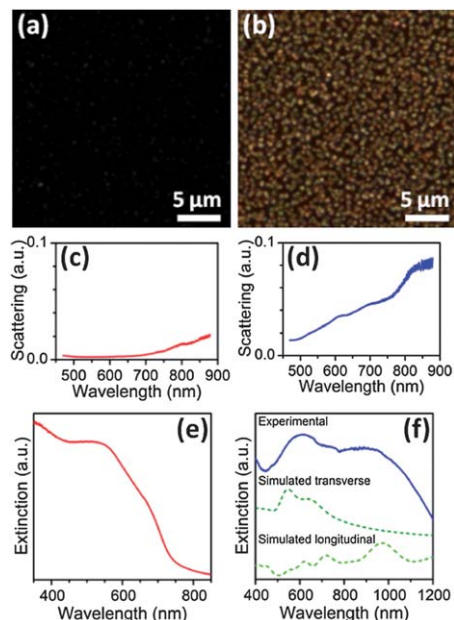

Fig. 2 SEM images of Au nanotube arrays with variable inner diameters and wall thicknesses of (a) ~200 nm and ~150 nm, respectively and (b) ~100 nm and ~30 nm, respectively. The insets in panels (a) and (b) show the corresponding magnified SEM images of single nanotubes, respectively (scale bar, 200 nm).

Fig. 4 Optical dark-field images of (a) CdSe nanotube arrays and (b) Au nanotube arrays on ITO/glass taken under the same condition (exposure time: 0.5 s). (c and d) The corresponding scattering spectra and (e and f) extinction spectra of the two nanotube arrays. In panel (f), the blue solid curve is the experimental extinction spectrum of Au nanotube arrays. The other two are simulated extinction spectra obtained from the FDTD calculations using the excitation light polarized perpendicular to the nanotube axis (dark green dashed curve) and parallel to the nanotube axis (light green dashed curve).

absorption with a sharp bandgap absorption edge at ~700 nm, agreeing well with the bandgap of CdSe (~1.7 eV ref. 39). The experimental extinction spectrum of Au nanotube arrays (blue solid curve in Fig. 4f) is rather different from that of the CdSe nanotube arrays, which exhibits a specific line profile with two broad peak features appearing at ~610 nm and ~890 nm. To understand the characteristic of the Au nanotube observed in the extinction spectrum, FDTD simulations were performed. As unpolarized light is employed in the experimental measurement of extinction spectra, the simulations were conducted with two different excitation polarizations, *i.e.*, the electric field of the incident light being perpendicular (transverse mode) to or parallel to (longitudinal mode) the axial direction of nanotube. A single nanotube with 100 nm inner diameter, 30 nm wall thickness, and 2000 nm length (which configuration is consistent with the typical Au nanotubes being measured experimentally) in vacuum was studied. The simulated spectra of the two polarization modes are shown in Fig. 4f (dark and light green dashed curves), qualitatively consistent with the experimental results. The peak at ~610 nm is predominantly contributed by the transverse localized surface plasmon resonance (LSPR), while the peak at ~890 nm mainly results from the longitudinal LSPR mode. The non-perfect match between the experimental and the simulated results might be originating from the non-uniform size and geometrical configuration of the nanotubes, the rough surface of tube walls, as well as the possible coupling effect that are not included in the simulation.
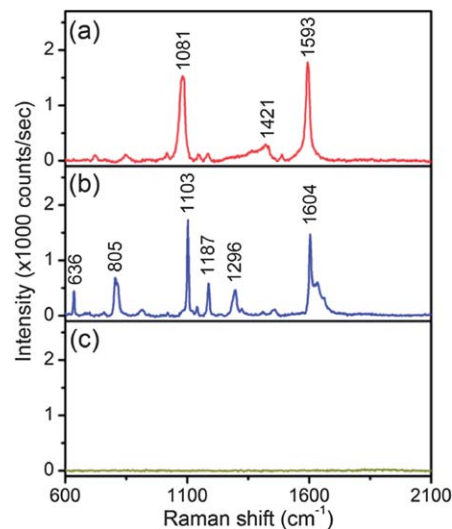

Fig. 5 Raman spectra of (a) 4-MBA molecules adsorbed on Au nanotube arrays on ITO/glass, (b) 4-MBA powder and (c) Au nanotube arrays.

Au nanotube arrays on ITO/glass as SERS substrates

The Raman spectrum of 4-MBA (a Raman-active molecule) adsorbed on Au nanotube arrays (Fig. 5a) exhibits two strong bands at ~1081 cm^{-1} and ~1593 cm^{-1}, as well as a weaker band at ~1421 cm^{-1}. The former two can be assigned to the ν(C=C) aromatic-ring-breathing modes and the latter one to the combination mode of ν(C=C) and δ(C–H).[40–44] No Raman peak is detected from Au nanotube arrays without 4-MBA coating under the same experimental conditions (Fig. 5c), indicating that all the observed peaks in Fig. 5a originate from the surface-enhanced Raman scattering of 4-MBA. However, compared to the Raman spectrum collected from 4-MBA powder (Fig. 5b), the Raman peaks are selectively enhanced when 4-MBA molecules are adsorbed onto the Au nanotube surface. Some of the peaks become weaker (*e.g.*, 1187 cm^{-1}) and some are missing (*e.g.*, 636, 805, and 1296 cm^{-1}). Moreover, the SERS peaks are also shifted several cm^{-1} and broadened with respect to those observed in the normal Raman spectrum. These changes observed in the SERS spectrum, consistent with the literature reports,[26,43,45,46] mainly result from the chemisorption of 4-MBA and the presence of a local electric field. The former alters the point group symmetry and vibrational modes of the molecules, and the latter modifies the peak intensities.[47] The enhancement factor estimated using the intensity of the ~1080 cm^{-1} band is around 4×10^4 (the details are given in the ESI†). This result is comparable to EFs obtained from other Au nanostructures.[26–29] For comparison, the SERS effect for Au-sputtered ITO/glass is much weaker (Fig. S5a†), due to its low local field enhancement.

Conclusions

In conclusion, large-scale Au nanotube arrays on the ITO substrate with tunable inner diameters and wall thicknesses have been successfully fabricated *via* CdSe nanotube array templating. The strong oxidation ability of AuCl$_4^-$ ions enables

the conversion of CdSe nanotubes to Au nanotubes while maintaining the tubular morphology. The extinction spectrum of Au nanotube arrays exhibits two major plasmonic peaks, which are mainly contributed by electron oscillation along the transverse and the longitudinal directions. Using the nanotube arrays as the SERS substrate, Raman scattering of 4-MBA is increased by approximately 4 orders of magnitude, ascribed to the plasmonic enhancement effect of the Au nanotube arrays.

Acknowledgements

Notes and references

1 T. K. Sau, A. L. Rogach, F. Jackel, T. A. Klar and J. Feldmann, *Adv. Mater.*, 2010, **22**, 1805.

2 K. L. Kelly, E. Coronado, L. L. Zhao and G. C. Schatz, *J. Phys. Chem. B*, 2003, **107**, 668.

3 X. H. Huang, S. Neretina and M. A. El-Sayed, *Adv. Mater.*, 2009, **21**, 4880.

4 J. Perez-Juste, I. Pastoriza-Santos, L. M. Liz-Marzan and P. Mulvaney, *Coord. Chem. Rev.*, 2005, **249**, 1870.

5 W. Ni, X. Kou, Z. Yang and J. F. Wang, *ACS Nano*, 2008, **2**, 677.

6 J. Zhu, *Mater. Sci. Eng., A*, 2007, **454**, 685.

7 A. Murphy, J. McPhillips, W. Hendren, C. McClatchey, R. Atkinson, G. Wurtz, A. V. Zayats and R. J. Pollard, *Nanotechnology*, 2011, **22**, 045705.

8 J. Yguerabide and E. E. Yguerabide, *Anal. Biochem.*, 1998, **262**, 137.

9 A. Wokaun, J. P. Gordon and P. F. Liao, *Phys. Rev. Lett.*, 1982, **48**, 957.

10 M. Delvaux, A. Walcarius and S. Demoustier-Champagne, *Anal. Chim. Acta*, 2004, **525**, 221.

11 X. Zhang, H. Wang, L. Bourgeois, R. Pan, D. Zhao and P. A. Webley, *J. Mater. Chem.*, 2008, **18**, 463.

12 M. D. Dickey, E. A. Weiss, E. J. Smythe, R. C. Chiechi, F. Capasso and G. M. Whitesides, *ACS Nano*, 2008, **2**, 800.

13 J. McPhillips, A. Murphy, M. P. Jonsson, W. R. Hendren, R. Atkinson, F. Hook, A. V. Zayats and R. J. Pollard, *ACS Nano*, 2010, **4**, 2210.

14 C. J. Brumlik and C. R. Martin, *J. Am. Chem. Soc.*, 1991, **113**, 3174.

15 C. J. Brumlik, V. P. Menon and C. R. Martin, *J. Mater. Res.*, 1994, **9**, 1174.

16 C. R. Martin, *Science*, 1994, **266**, 1961.

17 V. P. Menon and C. R. Martin, *Anal. Chem.*, 1995, **67**, 1920.

18 M. Nishizawa, V. P. Menon and C. R. Martin, *Science*, 1995, **268**, 700.

19 C. R. Martin, *Chem. Mater.*, 1996, **8**, 1739.

20 S. Demoustier-Champagne and M. Delvaux, *Mater. Sci. Eng., C*, 2001, **15**, 269.

21 M. A. Sanchez-Castillo, C. Couto, W. B. Kim and J. A. Dumesic, *Angew. Chem., Int. Ed.*, 2004, **43**, 1140.

22 W. R. Hendren, A. Murphy, P. Evans, D. O'Connor, G. A. Wurtz, A. V. Zayats, R. Atkinson and R. J. Pollard, *J. Phys.: Condens. Matter*, 2008, **20**, 362203.

23 T. Y. Shin, S. H. Yoo and S. Park, *Chem. Mater.*, 2008, **20**, 5682.

24 J. Kohl, M. Fireman and D. M. O'Carroll, *Phys. Rev. B: Condens. Matter Mater. Phys.*, 2011, **84**, 235118.

25 C. Mu, Y. X. Yn, R. M. Wang, K. Wu, D. S. Xu and G. L. Guo, *Adv. Mater.*, 2004, **16**, 1550.

26 N. J. Halas, S. Lal, W. S. Chang, S. Link and P. Nordlander, *Chem. Rev.*, 2011, **111**, 3913.

27 E. C. Le Ru, E. Blackie, M. Meyer and P. G. Etchegoin, *J. Phys. Chem. C*, 2007, **111**, 13794.

28 A. Campion and P. Kambhampati, *Chem. Soc. Rev.*, 1998, **27**, 241.

29 K. Kneipp, *Phys. Today*, 2007, **60**, 40.

30 M. J. Zhou, H. J. Zhu, X. N. Wang, Y. M. Xu, Y. Tao, S. Hark, X. D. Xiao and Q. Li, *Chem. Mater.*, 2010, **22**, 64.

31 M. Cocivera, A. Darkowski and B. Love, *J. Electrochem. Soc.*, 1984, **131**, 2514.

32 J. P. Szabo and M. Cocivera, *J. Electrochem. Soc.*, 1986, **133**, 1247.

33 J. H. Song, Y. Y. Wu, B. Messer, H. Kind and P. D. Yang, *J. Am. Chem. Soc.*, 2001, **123**, 10397.

34 B. Mayers, X. C. Jiang, D. Sunderland, B. Cattle and Y. N. Xia, *J. Am. Chem. Soc.*, 2003, **125**, 13364.

35 L. Carbone, S. Kudera, C. Giannini, G. Ciccarella, R. Cingolani, P. D. Cozzoli and L. Manna, *J. Mater. Chem.*, 2006, **16**, 3952.

36 R. Costi, A. E. Saunders, E. Elmalem, A. Salant and U. Banin, *Nano Lett.*, 2008, **8**, 637.

37 H. W. Liang, S. Liu, J. Y. Gong, S. B. Wang, L. Wang and S. H. Yu, *Adv. Mater.*, 2009, **21**, 1850.

38 H. M. Liu, B. M. Zeng and F. L. Jia, *Nanotechnology*, 2011, **22**, 305608.

39 M. Bouroushian, *Electrochemistry of Metal Chalcogenides*, Springer, 2010, p. 94.

40 P. Larkin, *Infrared and Raman spectroscopy: principles and spectral interpretation*, Elsevier Inc., 2011, pp. 86–93.

41 A. Michota and J. Bukowska, *J. Raman Spectrosc.*, 2003, **34**, 21.

42 C. J. Orendorff, A. Gole, T. K. Sau and C. J. Murphy, *Anal. Chem.*, 2005, **77**, 3261.

43 C. E. Talley, J. B. Jackson, C. Oubre, N. K. Grady, C. W. Hollars, S. M. Lane, T. R. Huser, P. Nordlander and N. J. Halas, *Nano Lett.*, 2005, **5**, 1569.

44 S. Z. Zhang, W. H. Ni, X. S. Kou, M. H. Yeung, L. D. Sun, J. F. Wang and C. H. Yan, *Adv. Funct. Mater.*, 2007, **17**, 3258.

45 C. Hrelescu, T. K. Sau, A. L. Rogach, F. Jackel and J. Feldmann, *Appl. Phys. Lett.*, 2009, **94**, 153113.

46 J. Kneipp, H. Kneipp, B. Wittig and K. Kneipp, *Nano Lett.*, 2007, **7**, 2819.

47 R. Aroca, *Surface-Enhanced Vibrational Spectroscopy*, John Wiley & Sons Ltd, 2006, pp. 73–106.

48 W. B. Cai, B. Ren, X. Q. Li, C. X. She, F. M. Liu, X. W. Cai and Z. Q. Tian, *Surf. Sci.*, 1998, **406**, 9.